JMEPEG (1997) 6:187-198

Mechanisms Governing Deformation and Damage during Elevated-Temperature Fatigue of an Aluminum-Magnesium-Silicon Alloy

T.S. Srivatsan, S. Anand, and N. Narendra

The cyclic deformation and fracture characteristics of aluminum alloy 6061 are presented and discussed. The specimens were cyclically deformed using fully reversed tension-compression loading under total strain-amplitude control, over a range of temperatures. The alloy showed evidence of softening to failure at all test temperatures. The degree of softening during fully reversed deformation increased with test temperature. The presence of shearable matrix precipitates results in a microstructure that offers a local decrease in resistance to dislocation movement, causing a progressive loss of strengthening contributions to the matrix. At elevated temperatures, localized oxidation and embrittlement at the grain boundaries are exacerbated by the applied cyclic stress and play an important role in accelerating crack initiation and subsequent crack propagation. The fracture behavior of the alloy is discussed in light of competing influences of intrinsic microstructural effects, deformation characteristics arising from a combination of mechanical and microstructural contributions, cyclic plastic strain amplitude and concomitant response stress, and the test temperature.

Keywords
Al6061-T651, aluminum alloy, fatigue, mechanisms, microstructure

1. Introduction

FOR MORE than three decades producers of aluminum have successfully developed and marketed a multitude of alloys and tempers to conform with the stringent demands of the aerospace and ground transportation industries. In fact, the sustained success achieved with the tried-and-true family of aluminum alloys has made designers reluctant to adopt alternative materials as viable replacements (Ref 1, 2). Aluminum alloys provide specific combinations of monotonic strength, stiffness, ductility, fracture toughness, fatigue crack initiation resistance, and fabricability. Their relatively high specific strength, coupled with low cost, good surface finish, corrosion resistance, and easy availability in a variety of forms, also has made these alloys an ideal choice for a spectrum of products.

Most experimental research studies have focused on understanding and improving the monotonic properties, cyclic fatigue resistance, fracture toughness, and overall fracture behavior of aluminum alloys through potentially viable alternatives of alloy design and innovative processing techniques aimed at achieving microstructural control. However, few studies have been performed to comprehensively understand the conjoint influence of elevated temperature and microstructure on cyclic stress response characteristics, cyclic strain resistance, low-cycle fatigue life, and deformation and fracture characteristics of precipitation-hardened aluminum alloys (Ref 3, 4).

Interest in cyclic stress and strain resistance is an important consideration in the design and operation of high-temperature systems that are subject to thermal stresses as a direct result of temperature transients that occur during start-up and shutdowns. Typical systems undergoing thermal transients include aircraft gas turbines, nuclear pressure vessels, steam turbines, and heat exchangers. Knowledge of cyclic stress/strain response is useful from the standpoint of understanding the response of metals to mechanical working, comprehending damage initiation and damage propagation characteristics, and engineering optimum microstructures for fatigue-sensitive and temperature-critical applications.

Information on the high-temperature strain-controlled low-cycle fatigue (LCF) behavior of aluminum alloys is relatively limited (Ref 3-5). Most research studies have focused on understanding room-temperature fatigue and fracture behavior (Ref 3-15).

The objective of this study was to systematically evaluate temperature influences on cyclic stress response characteristics and fracture behavior of aluminum alloy 6061 under fully reversed strain-amplitude-controlled cycling. The mechanisms and micromechanisms governing cyclic deformation and damage at elevated temperatures are explored. The cyclic stress response characteristics and low-cycle fatigue failure process are discussed in terms of the specific role of concurrent and mutually competitive influences of cyclic strain amplitude and resultant response stress, intrinsic microstructural effects, deformation characteristics of the matrix, test temperature, and macroscopic aspects of fracture.

2. Material and Experimental Techniques

2.1 *Material*

The aluminum alloy 6061 used in this study was manufactured and provided by the Aluminum Company of America. The nominal chemical composition of the alloy is given in Table 1. The alloy was investigated in the T651 condition (solution heat treated, quenched, stress relieved, and artificially aged to maximum strength).

T.S. Srivatsan, S. Anand, and **N. Narendra,** Department of Mechanical Engineering, The University of Akron, Akron, OH 44325-3903, USA.

2.2 *Experimental Techniques*

Fatigue test specimens were precision machined from the wrought plate with the stress axis parallel to the longitudinal direction (last rolling direction). The specimens were smooth and cylindrical in the gage section, which measured 6.25 mm in diameter and 25 mm in length. The chosen length-to-diameter ratio ensured that specimens would not buckle under fully reversed cyclic straining. To minimize the effects of surface irregularities and finish, final surface preparation was achieved by mechanically polishing the entire gage section of the test specimens to remove all circumferential scratches and surface machining marks.

The cyclic fatigue tests were performed on a fully automated, closed-loop servohydraulic structural test machine (Instron) equipped with a 10,000 kg (98 kN) load cell. The tests were conducted in the axial total strain-amplitude control mode under fully reversed, push-pull, tension-compression loading. For each individual test, the test machine was programmed to maintain a constant nominal strain rate of 0.001/s. The test

Table 1 Nominal composition of aluminum alloy 6061

Element	Weight percent
Magnesium	1.00
Silicon	0.60
Manganese	0.28
Chromium	0.20
Iron	trace
Aluminum	bal

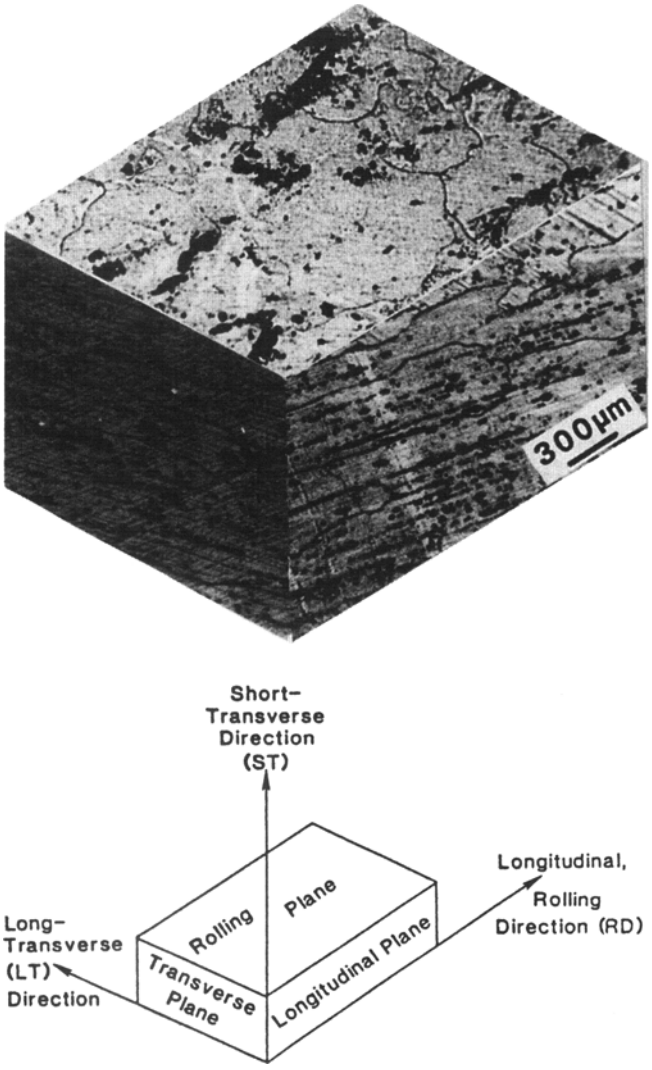

Fig. 1 Triplanar optical micrograph showing the grain structure of aluminum alloy 6061-T651 along the three orthogonal directions

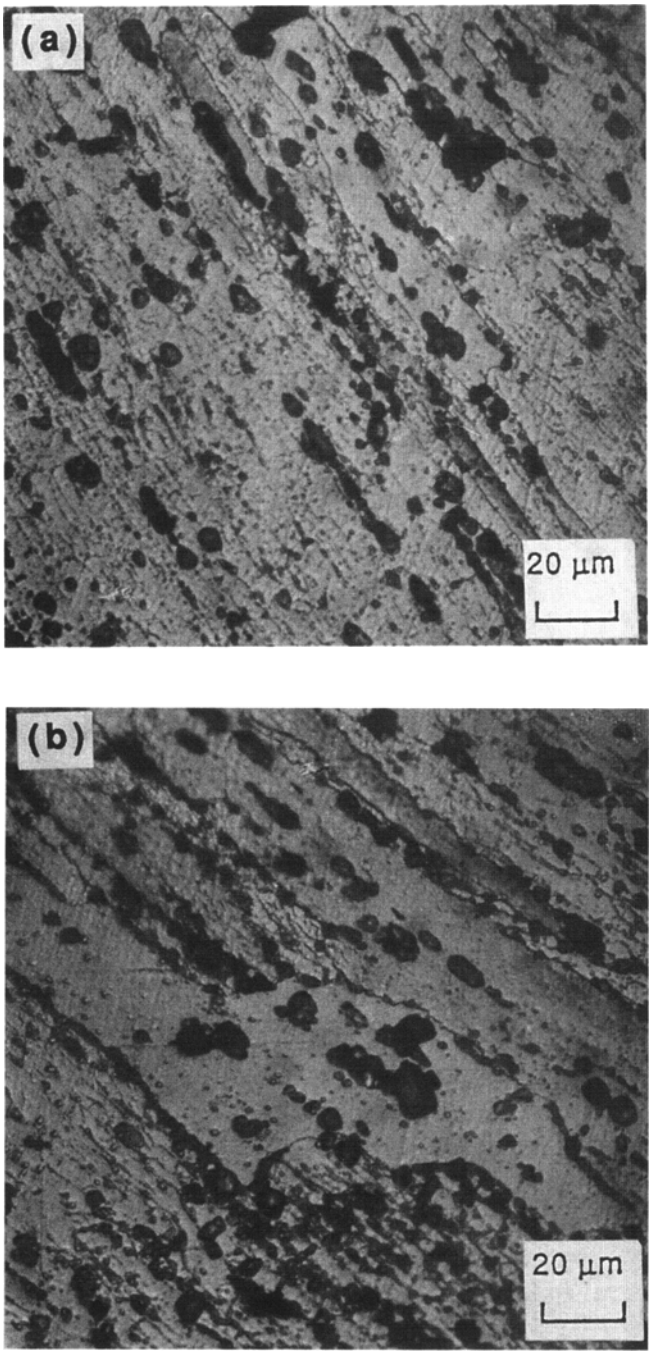

Fig. 2 Optical micrographs showing the distribution of coarse constituent and intermediate-size particles in the matrix (a) and at and along the grain-boundary regions (b)

command signal (strain function) exhibited a triangular waveform, and the mean strain was zero. All cyclic fatigue tests were initiated in tension.

An axial 12.7 mm gage length clip-on extensometer was attached to the test specimen at the gage section, using metal springs, to monitor the total strain amplitude during fully reversed strain-controlled fatigue tests such that the magnitude of negative strain equals the magnitude of positive strain [$R_\varepsilon = \varepsilon_{min}/\varepsilon_{max} = -1$]. The controlled variable is total strain amplitude [$\Delta\varepsilon_T/2$]. The extensometer was calibrated prior to the initiation of LCF testing.

The tests were conducted in controlled laboratory air environment (relative humidity, 55%) at ambient temperature (27 °C) and elevated temperatures (100 and 150 °C). The maximum test temperature (150 °C) corresponded to the temperature at which the alloy had been artificially aged to peak strength. The elevated-temperature tests were performed using an environmental chamber system unit (Instron Model 3111). The temperature was precisely controlled with the aid of a temperature controller linked to a thermocouple fixed on the surface of the specimen at the gage section. The elevated temperatures were within 2 °C of the setpoint over the entire duration of the test, and the temperature variation along the length of the test specimen was 2 °C. Ambient temperature varied from 28 to 30 °C during any given test.

For the elevated-temperature tests, the specimens were soaked or exposed to the temperature for 30 min prior to the initiation of testing. The hysteresis loops were recorded on a PC-based data acquisition system. The strain-amplitude-controlled LCF tests were performed at a constant total strain amplitude ($\Delta\varepsilon_T/2 = 0.70\%$). The tensile and compressive stresses were determined from the tips of the hysteresis loops. The number of cycles to failure or separation is taken as fatigue life (N_f).

The initial and final microstructures of the as-received 6061-T651 material were characterized by optical microscopy after standard metallographic preparation. Fracture surfaces of the deformed LCF test specimens were comprehensively examined in a scanning electron microscope (SEM) to determine the macroscopic fracture mode and to characterize the fine-scale topography and microscopic mechanisms governing LCF fracture. The distinction between macroscopic and microscopic fracture mechanisms is based on the magnification level at which the observations are made.

3. Results and Discussion

3.1 *Microstructure*

The microstructure of the as-received 6061-T651 alloy, shown in Fig. 1, is fully recrystallized with fairly large recrystallized grains. The presence of impurity elements, such as iron and silicon, results in the precipitation of a high volume fraction of coarse insoluble iron-rich and silicon-rich constituents during casting (Fig. 2). These large particles have been reported to be compounds of Al_7Cu_2Fe and $Al_{12}(FeMn)_3Si$ (Ref 16, 17). Their size ranges from 2 to 10 μm. The presence of the grain-refining element chromium results in intermediate-size dispersoids, which precipitate during ingot preheating and homogenization treatment (Ref 18). The coarse constituent particles and insoluble magnesium-rich phase (Al_2CuMg) were stratified and distributed along the rolling direction of the wrought plate. At frequent intervals, clustering or agglomeration of the coarse constituent and intermediate-size particles was observed (Fig. 2a). The particles were also found decorating the grain boundaries (Fig. 2b).

Strengthening in the alloy is due to the magnesium silicide (Mg_2Si) phase, which is the primary hardening precipitate formed during artificial aging of the alloy. A ratio of magnesium to available silicon of 1.7 to 1 ensures that all of the solute is contained in the Mg_2Si phase (Ref 19). The excess silicon in the alloy, over and above the amount required for the formation of the ordered Mg_2Si phase, is deposited at the grain boundaries as elemental silicon.

3.2 *Cyclic Stress Response*

Variation of cyclic stress with cycles (N), at a given temperature, is an important feature of the total strain-amplitude-controlled fatigue process. The stress response curves were determined by monitoring the cyclic stress amplitude ($\Delta\sigma/2$) during fully reversed strain-amplitude-controlled cycling. The stability of the intrinsic microstructural features during fully reversed cyclic straining and the intrinsic ability of the microstructure to homogeneously distribute or disperse the plastic strain are two important factors controlling the stress response characteristics of the material at a given test temperature.

The stress response curve, a plot of cyclic stress amplitude ($\Delta\sigma/2$) as a function of number of cycles (N) at a fixed total strain amplitude ($\Delta\varepsilon_T/2$), illustrates the path by which the material arrives at its final flow stress level. The stress response curves of alloy 6061-T651 are shown in Fig. 3. It is interesting to note that at all test temperatures the material shows continuous softening to failure from the onset of fully reversed cyclic deformation. At a constant total strain amplitude ($\Delta\varepsilon_T/2 = 0.70\%$), the overall degree of softening increased with an increase in test temperature; that is, the softening at 150 °C was greater than the softening observed at 100 °C, and the softening observed at 100 °C was more pronounced than the softening observed at ambient temperature (27 °C).

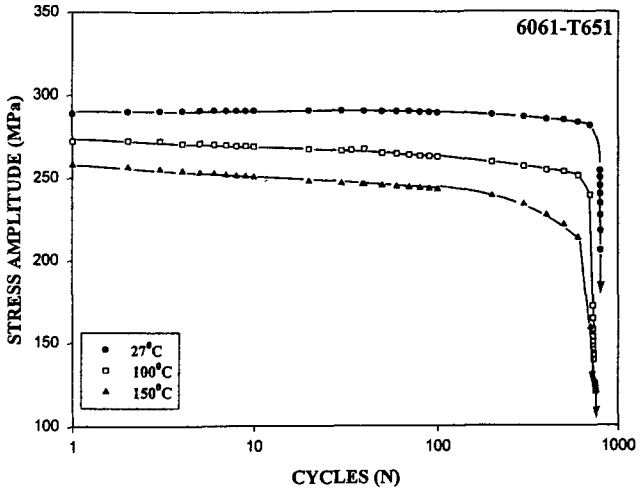

Fig. 3 Cyclic stress response curves for alloy 6061-T651

Fatigue life for a given microstructural condition is strongly dependent on test temperature and experimental conditions (cyclic strain amplitude). Figure 4 shows a comparison of the stress response behavior over the range of temperatures for a constant total strain amplitude of 0.70%. The stress amplitude ($\Delta\sigma/2$) is plotted as a function of fraction of life (N/N_f) to make comparison easier. It is apparent that the degree of softening increases with temperature and is far more pronounced at the higher test temperatures. The variation of normalized stress (σ_N/σ_1) with number of cycles (N) (Fig. 5) confirms the observation of an increase in softening with increase in test temperature. At a given temperature, the softening occurred by a progressive decrease in stress for both the tension and compressive parts of a strain-amplitude-controlled fatigue test (Fig. 6). This is easily distinguishable from the final crack-related softening, which occurs from an asymmetric decrease in load for the tensile part of the cycle.

The stress response curve can be considered to consist of three distinct stages: (1) rapid initial softening, (2) progressive softening for most of the fatigue life, and (3) a rapid decrease of stress culminating in catastrophic failure. The rapid decrease in stress is ascribed to the formation and presence of a number of microscopic cracks, which grow through the microstructure and eventually coalesce to form one or more macroscopic

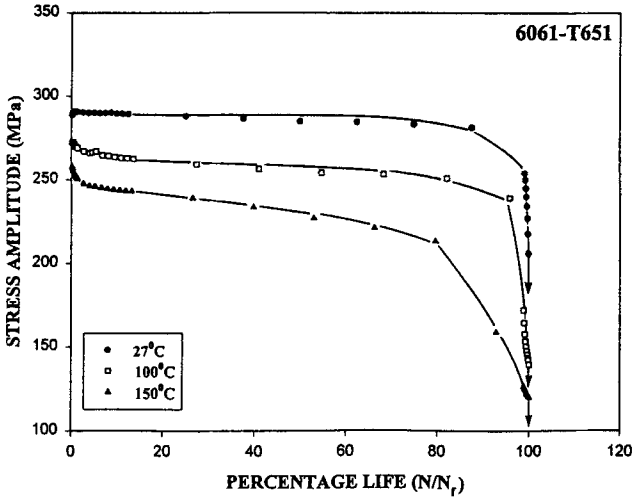

Fig. 4 Effect of test temperature on the cyclic stress response of alloy 6061-T651

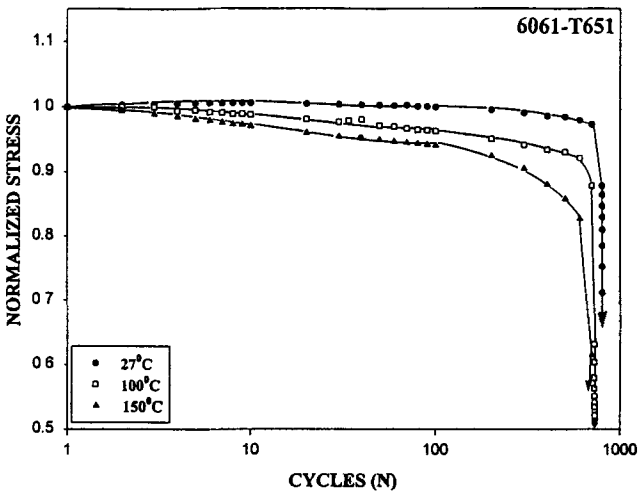

Fig. 5 Variation of normalized stress with fatigue cycles for alloy 6061-T651

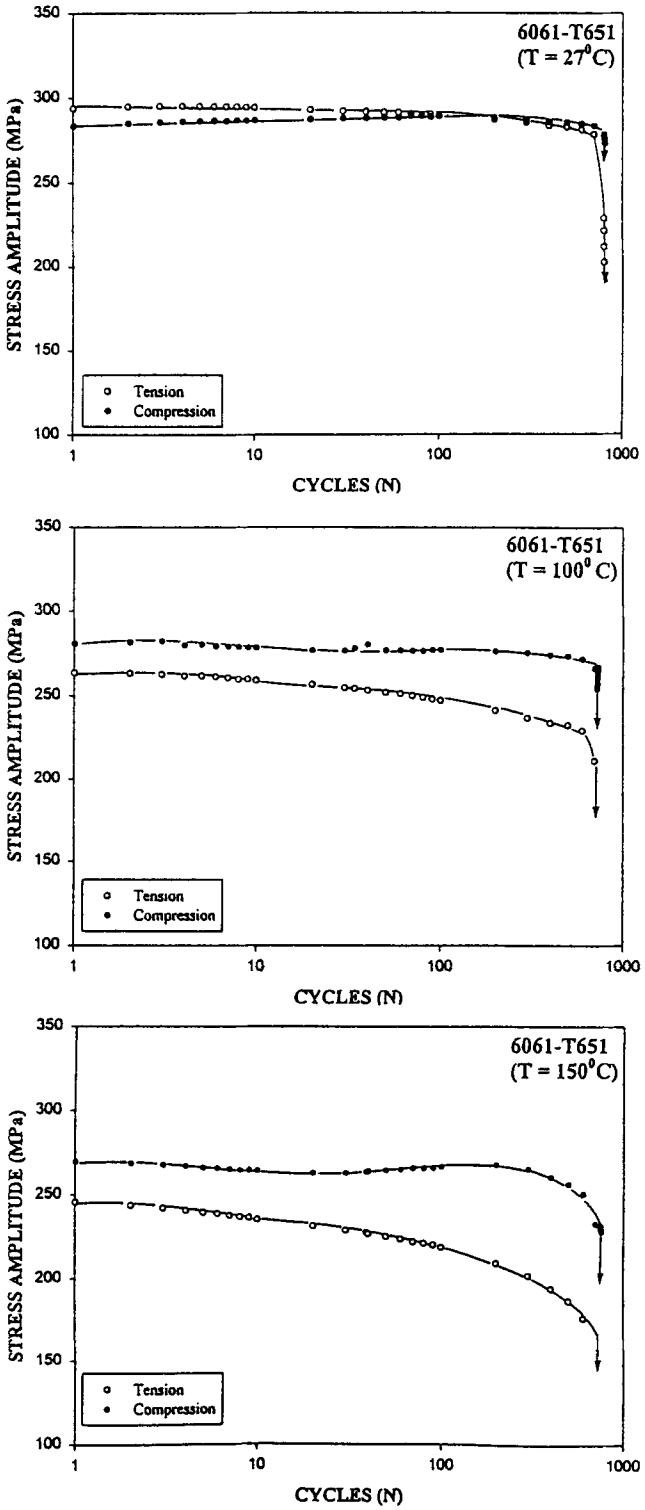

Fig. 6 Stress response curves showing the variation of tensile stress and compressive stress with cycles at a fixed total strain amplitude. (a) 27 °C. (b) 100 °C. (c) 150 °C

cracks. The softening effect is exacerbated by the concurrent growth of the fine microscopic and macroscopic cracks through the microstructure, coupled with progressive destruction of the intrinsic microstructural feature (strengthening precipitates and other second-phase inclusions) by the dislocation substructure. Cyclic plasticity, which is responsible for damage during fully reversed cyclic straining, increases with test temperature (Fig. 7). The increase in plastic strain amplitude ($\Delta\varepsilon_p/2$) with temperature follows an exponential trend.

3.3 *Mechanisms Governing Cyclic Deformation and Damage*

The intrinsic micromechanisms responsible for stress amplitude decrease and fatigue softening are dependent on the conjoint and mutually interactive influences of microstructure, cyclic strain range, and test temperature. The dominant strengthening mechanism for this aluminum alloy is precipitation hardening. Various mechanisms have been presented in the literature to explain the observed softening. Two key mechanisms are applicable for the aluminum-magnesium-silicon alloy 6061:

- Disordering of the strengthening precipitates by "mechanical scrambling"
- Reduction in size of the strengthening precipitate due to repeated shearing

During fully reversed cyclic straining, the to-and-fro motion of dislocations through the precipitate lattice causes a "scrambling" of the atoms of the strengthening precipitates (Mg_2Si). The general structure of the precipitate becomes disordered, and the probability of dislocation cutting (shearing) creating different atom pairs is progressively reduced. Disruption of the precipitate structure results in a progressive loss of contributions to strengthening with concomitant softening and the localization and/or accumulation of strain. The strain localization is either sufficient to cause structure disordering or becomes sufficient when accumulated over cycles.

At a given strain amplitude and concomitant response stress, the softening becomes pronounced when the strengthening precipitates have been sheared on a sufficient number of planes to result in a progressive degradation of the original precipitation-hardened microstructure within the persistent slip bands. Also, destruction of the strengthening precipitates causes the dislocations to pass on the active slip plane and the local work-hardening capability is progressively reduced. The slip bands are therefore intrinsically softer than the alloy, in its undeformed condition, primarily because hardening contributions by the second-phase particles are lost (Ref 20-22). Thus, a grain containing slip bands can be regarded as equivalent to a composite material consisting of a strong matrix in which is embedded thin planar lamellae of softer material. Since the two phases are subjected to the same far-field cyclic stress, the respective strains generated are radically different, resulting in inhomogeneous strain distribution and concomitant stress incompatibility at the slip band/matrix interfaces. This essentially results from the occurrence of plastic deformation in the slip bands, with the matrix subjected to only elastic deformation. In the cyclically deformed material, the overall distribution of strain appears to be inhomogeneous; some areas of the specimen show evidence of extensive deformation, or micro-

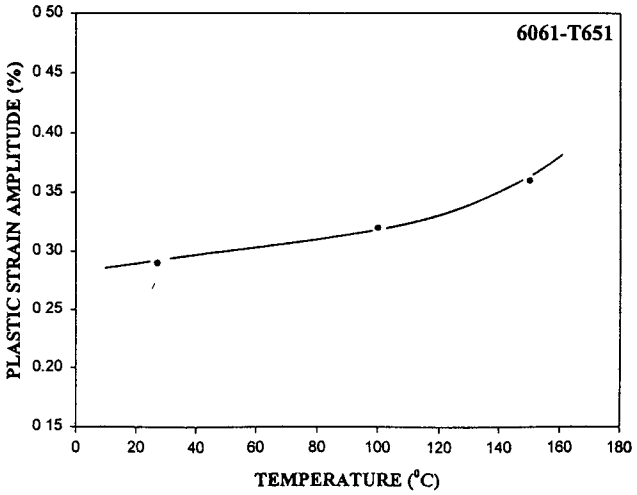

Fig. 7 Variation of cyclic plastic strain amplitude with test temperature

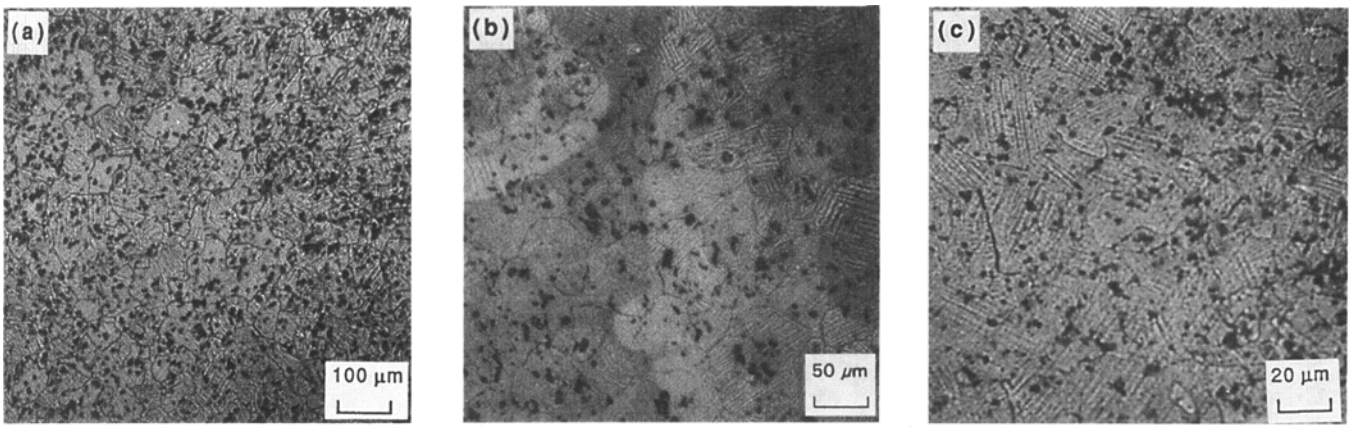

Fig. 8 Optical micrograph showing deformation structures in a sample cyclically deformed at a total strain amplitude of 0.70%. (a) 100 °C. (b) 150 °C

plasticity (Fig. 8), whereas others show limited or no deformation. The microplastic deformation resulting from the concentration of slip in specific bands and its nonuniform dispersion through the microstructure lead to inhomogeneous deformation (Fig. 8).

The localization of irreversible plastic strain within slip bands results in the buildup of dislocations at isolated points along the grain boundaries and at grain-boundary triple junctions. The associated high stress concentrations due to the dislocation pileup open intergranular cracks that propagate without absorbing much energy (Fig. 9). When local stress concentration (e.g., τ^*) exceeds the stress required for crack initiation at the grain boundaries, intergranular fracture is favored to occur (Ref 21). The presence of intergranular cracks increases with test temperature, with a concomitant reduction in cyclic strain resistance and LCF life. Also, impingement of the slip bands on the grain-boundary particles causes decohesion of their interface, resulting in the initiation of microscopic voids that progressively grow and coalesce to form microscopic cracks that propagate intergranularly. These observations are consistent with those reported in the literature on the detrimental influence of stress concentrations associated with planar slip band deformation. The increased softening observed in alloy 6060-T651 at the higher test temperatures results from the impingement of the planar deformation bands on grain boundaries and grain-boundary particles, and the resultant formation of microscopic cracks.

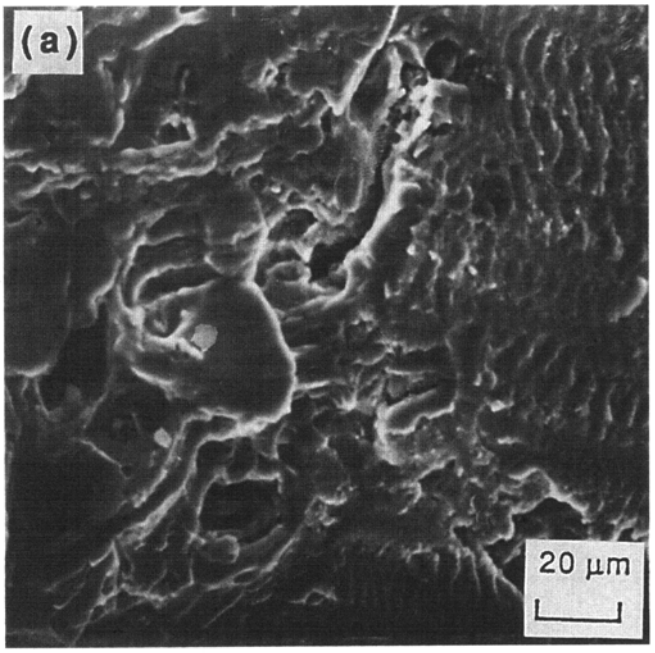

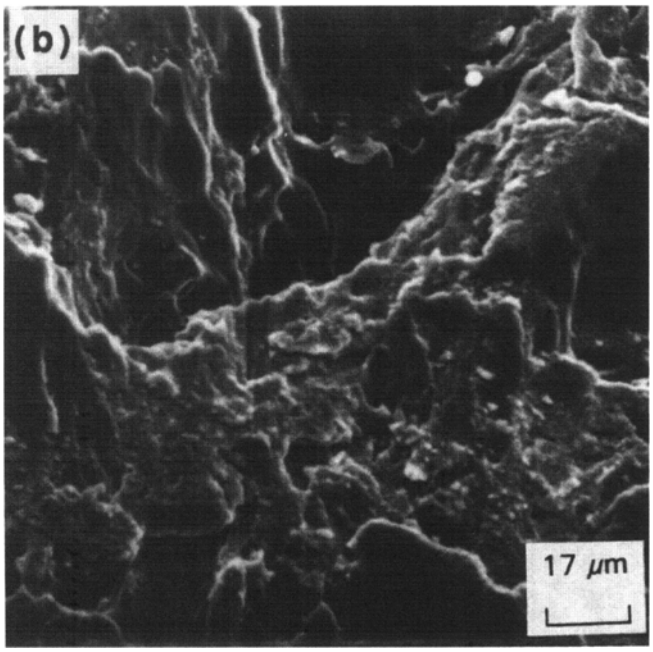

Fig. 9 SEM micrograph showing intergranular cracking in a sample cyclically deformed at 150 °C. (a) Along grain boundaries. (b) At grain-boundary triple junctions

Furthermore, the repeated shearing of the Mg_2Si strengthening precipitates in slip bands sets up a preferential path for the to-and-fro motion of dislocations during continued deformation of the material. Repeated shearing of the strengthening precipitates reduces their size until they offer little or no resistance to the movement of dislocations. Consequently, the stress necessary to shear the precipitates during repeated cycles is reduced, offering a resistance-free or precipitate-free path for the movement of dislocations. This phenomenon results in precipitate-free deformation bands and is largely responsible for the observed cyclic softening. The mechanical destruction of the strengthening precipitates and particles and the associated reduction in their size, coupled with the presence, growth, and eventual coalescence of the microscopic and macroscopic cracks, are viable explanations for the observed softening in alloy 6061-T651 during fully reversed strain cycling.

Low-cycle fatigue life is governed both by the initiation of fatigue cracks (damage) and by stage II propagation. The initiation consists of stage I crack propagation along crystallographic slip planes, whereas stage II propagation occurs, on average, in a direction normal to the applied cyclic stress. At the given total strain amplitude of 0.70%, the reduction in fatigue life at the higher test temperatures is mainly due to a decrease in the number of cycles spent in the initiation of fatigue cracks.

The potentially viable mechanisms responsible for the "damage" at elevated temperatures are summarized in Fig. 10. It is assumed that alloy 6061-T651 has an intrinsic ability to sustain a certain amount of damage prior to failure. Such damage can be the result of any one or a combination of these effects (Ref 23):

1 Deformation debris associated with the motion of dislocations
2 Metallurgical changes associated with coarsening and formation of new phases
3 Interactions between 1 and 2

The damage tolerance capability of the microstructure is largely dependent on the damage accumulation mechanism. Other competing mechanisms contributing to damage during

fully reversed strain cycling, particularly at elevated temperatures, are oxidation and embrittlement.

The principal strengthening precipitates Mg_2Si are ordered and thermodynamically stable for a prolonged period of time at a particular test temperature, and up to test temperatures that are much higher than those used in this study. Considering the limited time duration of each strain-amplitude-controlled fatigue test, in comparison with the time actually required to bring about metallurgical transformations through the development of new phases and coarsening of the precipitate particles, this damage mechanism can be ruled out.

Various creep mechanisms can be unduly damaging when compared to the other deformation modes. In the present case, the wave shape effect resulting from cycling with unbalanced hysteresis loops and the intrinsic micromechanisms that promote and enhance grain-boundary degradation are important and must be considered. Since aluminum alloy 6061 was subjected to balanced hysteresis loop cycling—that is, equal ramp rates for each leg—damage from creep due to the effect of unbalanced cycling does not arise. Creep damage due to enhanced grain-boundary degradation is also ruled out; fractographic observations of the samples deformed to failure at the different temperatures showed that the degradation in cyclic fatigue life at the higher test temperatures did not occur as a result of a drastic change in fracture mode from predominantly ductile transgranular to brittle intergranular failure. The occurrence of plastic strain inhomogeneity aided by grain-boundary particles is believed to be responsible for the observed intergranular cracking (Fig. 9). Besides, the short period of the associated with each total strain-amplitude-controlled fatigue test, at the elevated temperatures, is insufficient to cause any significant time-dependent damage due to creep.

The detrimental effects of water vapor during cyclic fatigue at ambient temperature and in moist air environments are fairly well documented (Ref 24-30). In elevated-temperature applications, however, the effect of oxidation is of primary concern, and environmental damage due to this effect under balanced hysteresis loop cycling has been documented by other researchers in independent studies (Ref 31-33). Oxidation is a time-dependent process controlled by two important parameters: availability of oxygen and solid-state diffusion rates. The normal processes of crack initiation and growth that occur at ambient temperature (27 °C) are accelerated in the hostile laboratory air environment at the higher test temperatures. The freshly exposed surfaces that are produced by local plastic deformation are rapidly oxidized and aid in localizing the strain. This results in further rupturing and localization, which directly aids in reducing the time period normally associated with crack initiation. On occasion, the oxide completely bridges the surface cracks, resulting in a local increase in the intrinsic load-bearing capability of the specimen. Of the several different possibilities, the following factors can be considered instrumental in accelerating fatigue damage and degrading the cyclic strain resistance and overall fatigue life of alloy 6061-T651 in the hostile laboratory air environment:

- Absorption of oxygen from the environment and occurrence of oxidation at and around the immediate vicinity of the crack tip
- Segregation of reactive elements in the environment, such as moisture and oxygen, to grain boundaries ahead of the propagating crack tip
- The inherent chemical complexity of grain boundaries, which results in preferential oxidation along them and

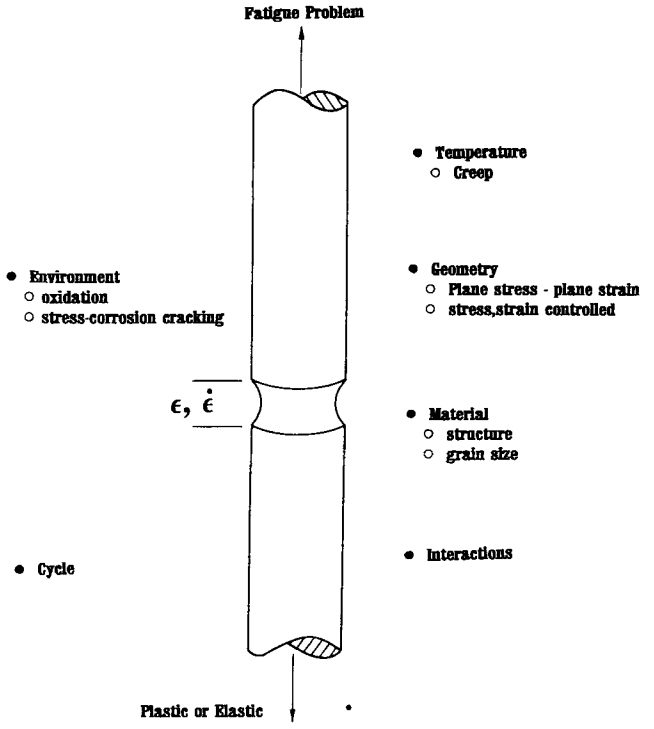

Fig. 10 Schematic showing the important variables during high-temperature LCF

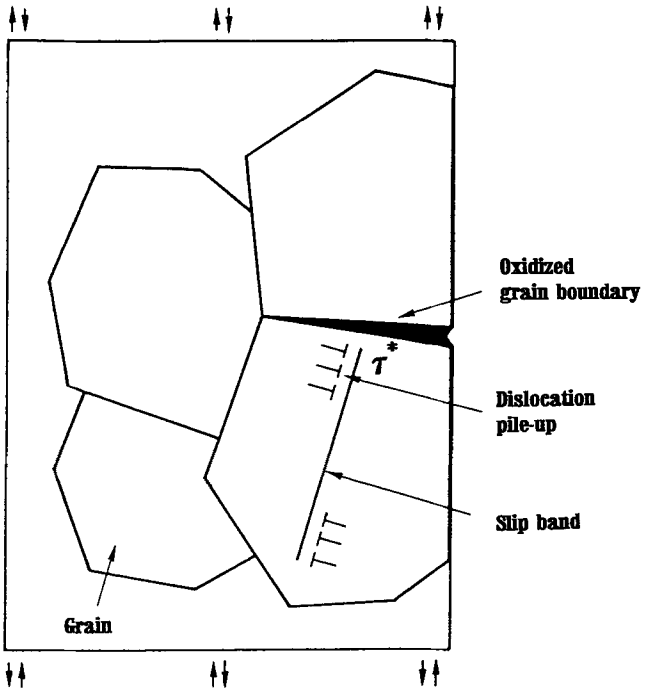

Fig. 11 Schematic of the embrittlement mechanism showing the intersection of a persistent slip band with an oxidized grain boundary

along the slip bands. Grain-boundary oxidation ahead of an advancing crack considerably weakens the boundary and facilities intergranular grain-boundary crack propagation.

- Cracking of the oxide at the crack tip, under the influence of applied cyclic stress and strain, and the subsequent formation of oxide at the freshly exposed metal. This contributes to enhancement of crack growth, with a concomitant reduction in cyclic fatigue life.

At the elevated temperatures, nucleating mechanisms arising from metal/environment interactions are exacerbated in the environment of laboratory air. Oxide formation and concurrent rupturing contribute to an increase in the length of the microscopic crack, thereby facilitating a local increase in crack propagation rate with a resultant reduction in cyclic endurance.

A reduction in cyclic fatigue life arising from increased softening also results from deformation/environment interactions or embrittlement. A progressive embrittlement of the boundary is favored since the microstructure of the alloy is such that the planar motion of dislocations during plastic deformation is not interrupted by the Mg_2Si strengthening precipitates in the microstructure. The embrittlement process is a complex

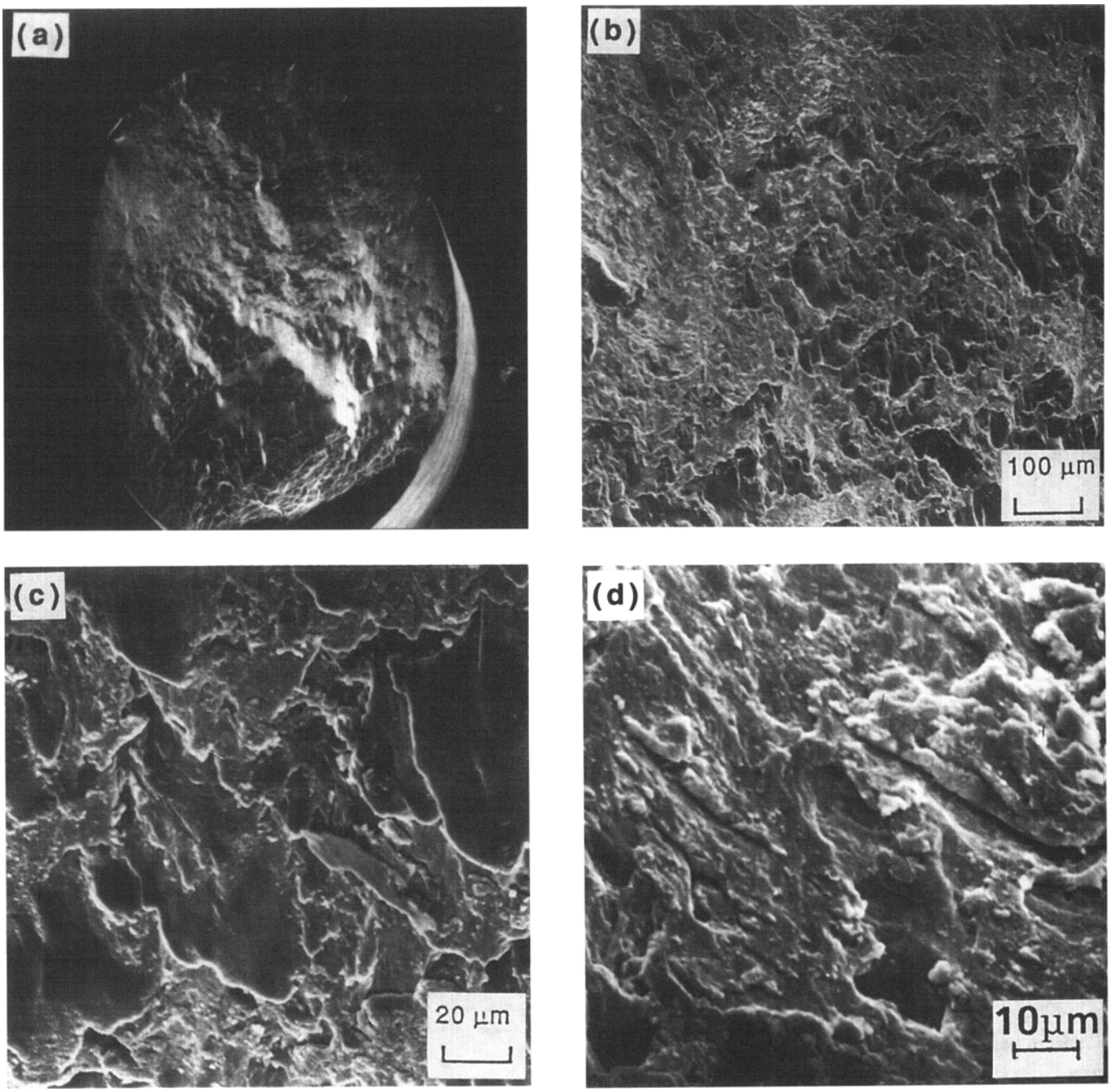

Fig. 12 SEM micrographs of the LCF fracture surface of a sample deformed at ambient temperature, N_f = 802 cycles. (a) Overall morphology. (b) High-magnification view of (a). (c) Tear ridges and microscopic cracks. (d) Microscopic cracks

interaction of precipitate structure, microstructure (grain size), mechanical properties (such as strength and toughness), environment, and test temperature (Fig. 11). The embrittlement of the grain boundary is a key factor that contributes to the degradation in fatigue resistance experienced at the elevated temperatures as well as damage caused by cyclic plastic strain. The enhancement of both oxidation and embrittlement, by the applied cyclic stress, results from any one or mutually interactive influences of:

- Disruption of surface integrity by the emergence of dislocations
- Increase in chemical potential of the atoms in a shear stress field
- Enhancement of local atomic mobility as a direct result of dislocation concentrations
- Expansion of the crack in tension, providing room for the formation of oxides

3.4 *Fracture Behavior*

The LCF fracture surface features of alloy 6061 were examined at low magnification to identify the fatigue and overload (final fracture) regions, and at higher magnifications in the fatigue region to identify regions of crack initiation and early microscopic crack growth (i.e., region of stable crack growth). Samples for SEM were obtained from the deformed fatigue specimens by sectioning parallel to the fracture surface. Fracture surfaces revealed near-similar topographies at the different temperatures. Representative fractographs are shown in Fig. 12 to 14.

3.4.1 Ambient Temperature (27 °C)

The fracture surface of the specimen cyclically deformed at ambient temperature with a total strain amplitude of 0.70%, on a macroscopic scale, was at 60° with respect to the major stress axis. Distinct regions of stable and unstable crack growth were apparent. Fracture in the region of unstable crack growth and overload was bimodal, comprising regions of transgranular and intergranular failure.

The region of stable microscopic crack growth was essentially featureless (Fig. 12a). High-magnification observations of this area revealed ridges dispersed in a transgranular region (Fig. 12b). The region of early crack growth—that is, the region between the surface and the overload (unstable crack growth)—revealed pronounced cracking along the grain boundaries (Fig. 12d). The intergranular cracks were parallel to the major stress axis.

The tendency toward localized nonhomogeneous (planar) deformation and the termination of the dislocation bands at grain boundaries results in the localization of strain with concomitant stress concentrations in these regions. This is exacerbated by the presence of undissolved iron-rich and silicon-rich intermetallics and insoluble magnesium-rich constituent phases at and near the grain boundary regions, and is a plausible explanation for the observed intergranular fracture mode. The observed nonlinearity (small deflections and bifurcations) of the microscopic and macroscopic cracks is attributed to slip planarity. The overload region revealed voids of varying size and shallow dimples.

3.4.2 Temperature: 100 °C

Fatigue fracture at 100 °C was at 45° with respect to the major stress axis (Fig. 13a) and revealed distinct regions of stable crack growth and overload. The region of early microscopic crack growth was relatively smooth (Fig. 13b) and comprised numerous voids of varying size distributed randomly throughout the surface (Fig. 13c). Numerous fine microscopic cracks were observed in the direction parallel to the major stress axis (Fig. 13d). The overload region revealed a bimodal distribution of voids and dimples, as well as numerous fine microscopic cracks, features reminiscent of classical ductile and brittle failure (Fig. 13d).

3.4.3 Temperature: 150 °C

On a macroscopic scale, fatigue fracture at 150 °C occurred along a plane inclined at 45° with respect to the stress axis, following a plane of maximum macroscopic shear stress (Fig. 14a). However, the fracture surface was relatively rough when viewed at the microscopic level. The region of stable crack growth was transgranular and comprised a random distribution of microscopic voids. The region between stable and unstable crack growth revealed a bimodal distribution of voids and numerous fine microscopic cracks (Fig. 14b). High-magnification observations in the region of stable crack growth revealed striationlike features indicative of stable crack propagation (Fig. 14c). The overload region revealed numerous voids of varying size and shape (Fig. 14d).

3.4.4 Summary

The coarse iron-rich and silicon-rich constituent particles and traces of magnesium-rich insoluble phases tend to either crack easily because of their intrinsic brittleness or decohere at their interfaces (Ref 34-36). Interfacial strength is a dominant factor in the nucleation of the microscopic voids. Other factors that exert a profound influence on void initiation and growth include (Ref 36, 37): (1) size of the second-phase particles, (2) particle shape, (3) location and volume fraction, and (4) intrinsic strength of the particle.

Void initiation at the coarse constituent and other large second-phase particles in the microstructure is also influenced by the interactive influences of local stress and strain levels, and by the deformation mode. The presence of numerous coarse constituent particles and insoluble phases, coupled with a matrix microstructure that promotes localized inhomogeneous deformation, facilitates the nucleation of voids at relatively low to moderate stresses. In fact, void initiation at a coarse second-phase particle occurs when the elastic energy in the particle exceeds the surface energy of the newly formed void surfaces (Ref 36). Simultaneously, the intermediate-size chromium-containing dispersoids present in the microstructure decrease the energy required to propagate the crack, aiding in the initiation of microscopic voids that coalesce to form void sheets and thereby facilitating linking of the microscopic cracks initiated at the grain-boundary regions and the coarse constituent particles. The larger voids, which were created by fracture of the coarse and intermediate-size constituent particles, coalesce by impingement. The more widely separated voids were found to coalesce by the formation of void sheets. The halves of the fine

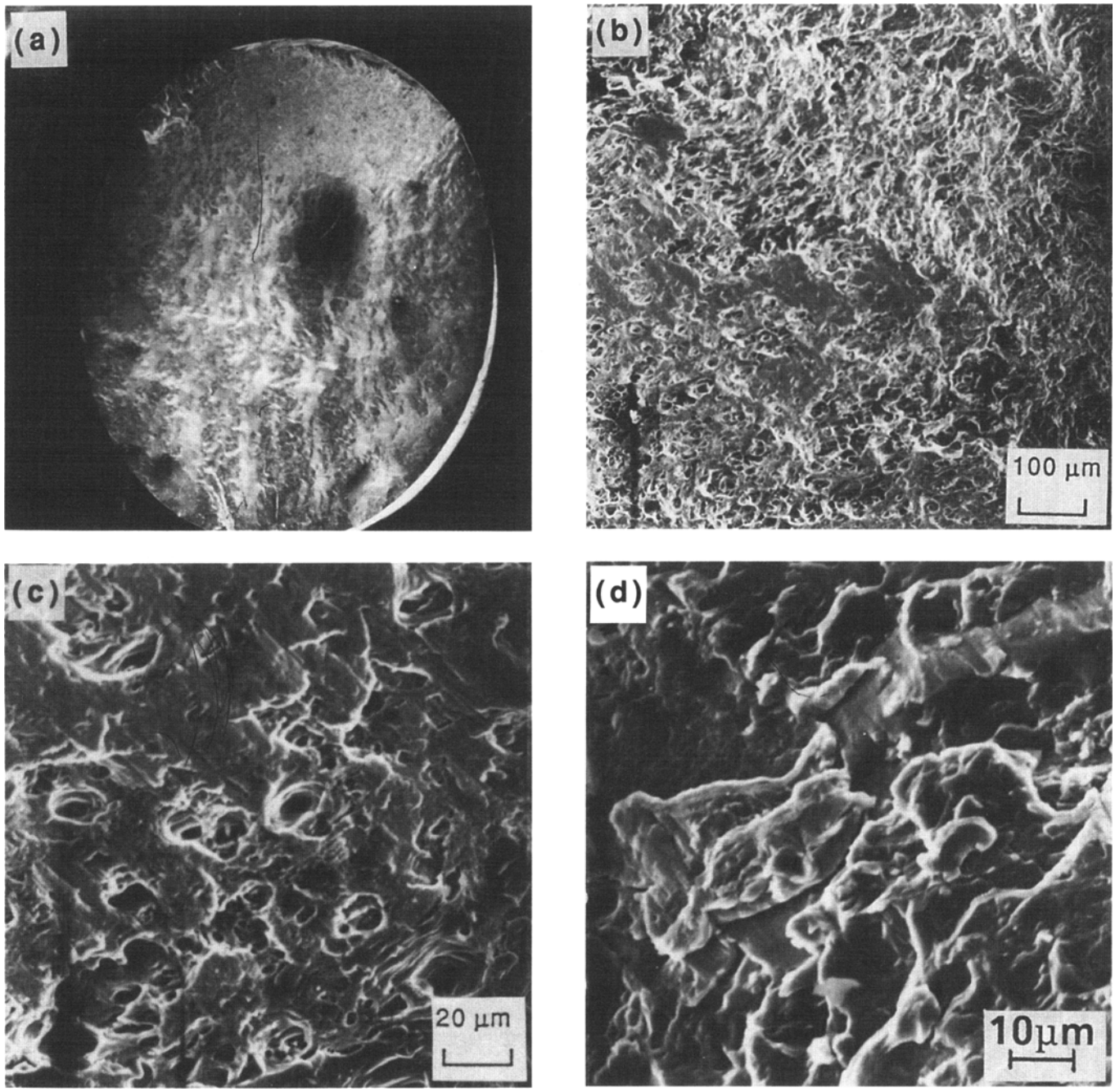

Fig. 13 SEM micrographs of the LCF fracture surface of a sample deformed at 100 °C, N_f = 732 cycles. (a) Overall morphology. (b) High-magnification view of (a) showing featureless region of stable crack growth. (c) Higher-magnification view of (b). (d) Region of unstable crack growth showing microscopic cracking and voids

microscopic voids are the shallow dimples visible on the fatigue fracture surface of alloy 6061-T651.

4. Conclusions

This comprehensive study of the mechanisms governing deformation and damage during elevated-temperature fatigue of aluminum alloy 6061 revealed a number of observations.

The microstructure of the as-received alloy was recrystallized with large recrystallized grains. Numerous coarse constituent particles were stratified and distributed along the rolling direction of the wrought plate. Clustering or agglomeration of the particles occurred at frequent intervals.

Cyclic stress response of the alloy containing fine matrix precipitates and a large number of coarse and intermediate-size particles revealed softening to failure from the onset of fully reversed straining. This is aided by the growth and coalescence of the microscopic cracks to form one or more macroscopic

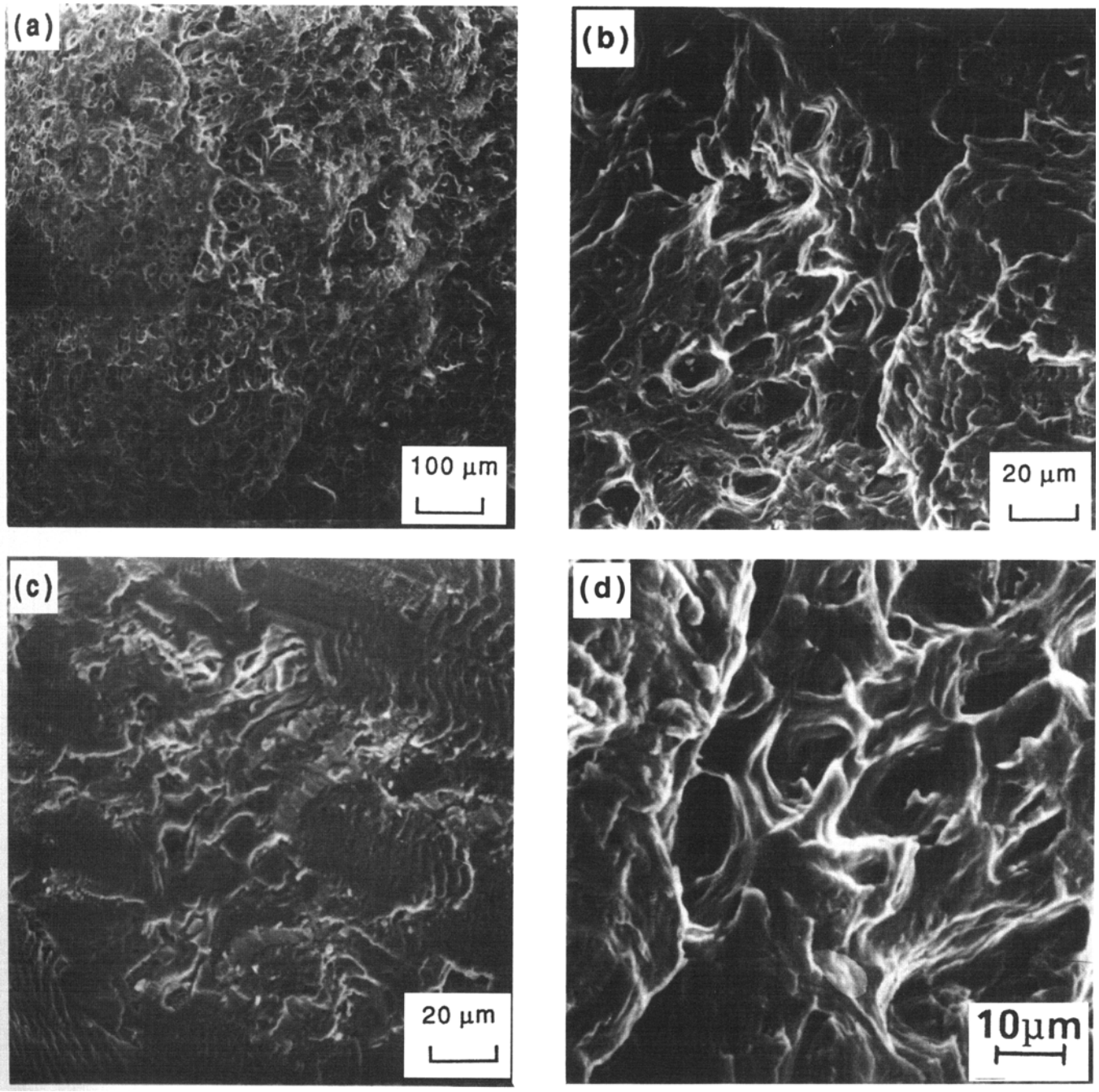

Fig. 14 SEM micrographs of the LCF fracture surface of a sample deformed at 150 °C, N_f = 755 cycles. (a) Region of stable crack growth. (b) High-magnification view of (a). (c) Striationlike features in region of stable crack growth. (d) Macroscopic and microscopic voids in the region of overload

cracks and a progressive decrease in the stress-carrying capability or softening of the structure. The overall degree of softening increased with an increase in test temperature.

The mechanism responsible for the decrease in stress amplitude during fully reversed strain-amplitude-controlled cycling is a progressive deterioration of strengthening contribution to the matrix caused by an interaction of dislocations with the strengthening precipitates and second-phase particles. The inhomogeneous deformation resulting from dislocation/precipitate interactions results in the localization of strain at the grain-boundary regions and concomitant intergranular deformation.

The short period of time associated with each LCF test when compared to the actual time required to cause any time-dependent damage rules out the possibility of creep as a contributing factor. At the elevated temperatures, localized oxidation and embrittlement are major contributors to fatigue damage. The formation of oxides at the higher test temperatures, and their repeated rupturing during fully reversed cyclic straining, contributes to a local increase in crack length and enhances the rate of

crack propagation and thus softening. Embrittlement results from the conjoint influence of mechanisms involving intrinsic microstructural features, material strength and ductility, and the nature of the environment. The synergistic influence of these mechanisms on cyclic response is exacerbated by the applied stress.

Cyclic fracture morphology was essentially similar at the different temperatures. Fracture was bimodal, comprising distinct regions of stable and unstable crack growth. In the intergranular regions, the crack followed the grain boundaries. The microscopic crack path through the microstructure was tortuous, with evidence of deflections during propagation. The region of unstable crack growth comprised numerous voids, shallow dimples, and microscopic cracks—features reminiscent of locally ductile and brittle failure.

Acknowledgment

The authors thank the University of Akron for partially supporting this research study.

References

1. J.T. Staley and D.J. Lege, *J. Phys. IV,* Vol 3, 1993, p 179
2. J.T. Staley, Aluminum Alloys and Composites, *Encyclopedia of Physical Science,* Vol 1, 1992, p 591
3. T.S. Srivatsan, *Int. J. Fatigue,* Vol 10 (No. 2), 1988, p 91
4. T.S. Srivatsan, K. Yamaguchi, and E.A. Starke, Jr., *Mater. Sci. Eng.,* Vol 83, 1986, p 87-107
5. T.S. Srivatsan, V.K. Vasudevan, and D. Veeraraghavan, Cyclic Strain Resistance and Fracture Behavior of Aluminum Alloy 7055, *Eng. Fract. Mech.,* submitted for publication
6. R.E. Sanders, Jr. and E.A. Starke, Jr., *Mater. Sci. Eng.,* Vol 28, 1977, p 53
7. R.E. Sanders, Jr. and E.A. Starke, Jr., *Metall. Trans.,* Vol 9A, 1978, p 1087
8. T.H. Sanders, Jr. and E.A. Starke, Jr., *Metall. Trans.,* Vol 7A, 1976, p 1107-1117
9. T.S. Srivatsan and E.J. Coyne, Jr., *Int. J. Fatigue,* Vol 8 (No. 4), 1986, p 201
10. T.S. Srivatsan, *Int. J. Fatigue,* Vol 13 (No. 4), 1991, p 313-321
11. T.S. Srivatsan, D. Lanning, and K.K. Soni, *Int. J. Fatigue,* Vol 15 (No. 3), 1993, p 231-242
12. T.S. Srivatsan, T. Hoff, and A. Prakash, *Eng. Fract. Mech.,* Vol 40 (No. 2), 1991, p 297-309
13. T.S. Srivatsan and D. Lanning, Jr., *Eng. Fract. Mech.,* Vol 42 (No. 5), 1992, p 877-892
14. T.S. Srivatsan, S. Sriram, and C. Daniels, Influence of Temperature on Cyclic Stress Response and Fracture Behavior of Aluminum Alloy 6061, *Eng. Fract. Mech.,* Vol 51, 1997, in press
15. T.S. Srivatsan and V.K. Vasudevan, Cyclic Plastic Strain Response and Fracture Behavior of 2080 Aluminum Alloy Metal-Matrix Composite, *Int. J. Fatigue,* 1997, in press
16. A.K. Vasudevan, R.D. Doherty, and S. Suresh, in *Aluminum Alloys: Contemporary Research and Applications,* A.K. Vasudevan and R.D. Doherty, Ed., *Treatise in Materials Science and Technology,* Vol 31, Academic Press, 1989, p 446
17. E.A. Starke, Jr., in *Aluminum Alloys: Contemporary Research and Applications,* A.K. Vasudevan and R.D. Doherty, Ed., *Treatise in Materials Science and Technology,* Vol 31, Academic Press, 1989, p 35
18. E.A. Starke, Jr. and G. Lutjering, in *Fatigue and Microstructure,* M. Meshii, Ed., American Society for Metals, 1979, p 205
19. T.S. Srivatsan, C.W. Meyers, and J.T. Berry, *J. Test. Eval.,* Vol 15, 1987, p 196
20. C. Calabrese and C. Laird, *Mater. Sci. Eng.,* Vol 13, 1974, p 159-170
21. J.M. Duva, M.A. Daeubler, E.A. Starke, Jr., and G. Lutjering, *Acta Metall.,* Vol 36 (No. 3), 1988, p 585
22. W.J. Baxter and T.R. McKinney, *Metall. Trans.,* Vol 19A, 1988, p 83
23. S.D. Antolovich, in *La Fatigue des Materiaux et des Structures,* C. Bathias and J.P. Bailon, Ed., Mailoine, Paris, 1980, p 465
24. J.H. Gough and D.G. Sopwith, *J. Inst. Met.,* Vol 72, 1946, p 465
25. N. Thompson, N.J. Wadsworth, and N. Louat, *Philos. Mag.,.* Vol 1, 1956, p 113
26. N.J. Wadsworth and J. Hutchings, *Philos. Mag.,* Vol 3, 1969, p 1154
27. M.R. Achter, in *STP 415,* ASTM, 1967, p 181
28. R.H. Cook and R.P. Skelton, *Int. Met. Rev.,* Vol 19, 1974, p 187-199
29. T.S. Srivatsan and T.S. Sudarshan, *Eng. Fract. Mech.,* Vol 36 (No. 6), 1990, p 827-852
30. T.S. Srivatsan and T.S. Sudarshan, *J. Mater. Sci.,* Vol 23, 1988, p 1521-1533
31. S.S. Manson and R. Zab, in *Environmental Degradation of Engineering Materials,* M.R. Louthan, Jr. and R.P. McNitt, Ed., Virginia Polytechnic Institute Press, 1977, p 754
32. D. Fournier and A. Pineau, *Metall. Trans.,* Vol 8A, 1977, p 1095
33. M. Prager and G. Sines, "Embrittlement of Precipitation Hardenable Nickel-Base Alloys," Paper No. 71, American Society of Mechanical Engineers, 1971
34. J. Gurland and J. Plateau, *Trans. ASM,* Vol 56, 1963, p 442
35. R.H. Van Stone and J.A. Psioda, *Metall. Trans.,* Vol 6A, 1975, p 672
36. R.H. Van Stone, T.B. Cox, J.R. Low, Jr., and J.A. Psioda, *Int. Met. Rev.,* Vol 30, 1985, p 157
37. A.S. Argon, J. Im, and R. Safoglu, *Metall. Trans.,* Vol 6A, 1975, p 825